

**Influence of moisture condition on chloride diffusion in partially saturated ordinary Portland cement mortar**

Zhang, Yong; Zhang, Mingzhong; Ye, Guang

**DOI**

[10.1617/s11527-018-1162-7](https://doi.org/10.1617/s11527-018-1162-7)

**Publication date**

2018

**Document Version**

Final published version

**Published in**

Materials and Structures

**Citation (APA)**

Zhang, Y., Zhang, M., & Ye, G. (2018). Influence of moisture condition on chloride diffusion in partially saturated ordinary Portland cement mortar. *Materials and Structures*, 51(2), Article 36. <https://doi.org/10.1617/s11527-018-1162-7>

**Important note**

To cite this publication, please use the final published version (if applicable). Please check the document version above.


**Copyright**

Other than for strictly personal use, it is not permitted to download, forward or distribute the text or part of it, without the consent of the author(s) and/or copyright holder(s), unless the work is under an open content license such as Creative Commons.

**Takedown policy**

Please contact us and provide details if you believe this document breaches copyrights. We will remove access to the work immediately and investigate your claim.

# Influence of moisture condition on chloride diffusion in partially saturated ordinary Portland cement mortar

Yong Zhang  · Mingzhong Zhang · Guang Ye

Received: 3 October 2017 / Accepted: 8 February 2018  
© The Author(s) 2018. This article is an open access publication

**Abstract** Experiments have been carried out to study the influence of moisture condition, including moisture content and its distribution, on the chloride diffusion in partially saturated ordinary Portland cement mortar. The mortar samples with water-to-cement ( $w/c$ ) ratios of 0.4, 0.5 and 0.6, cured for 1 year, were preconditioned to uniform water saturations ranging from 18 to 100%. The interior relative humidities of these partially saturated cement mortars, i.e. water vapour desorption isotherm (WVDI), were measured. The WVDI results in relation to the pore structures obtained from the mercury intrusion porosimetry tests of paste samples with the same  $w/c$  ratios were analyzed, which provided a basic insight into the moisture distribution in the non-saturated cement mortars. The relative chloride diffusion coefficients of cement mortars at various water saturations were determined based on the Nernst-Einstein equation and conductivity technique. It is found that the

relative chloride diffusion coefficient  $D_{rc}$  depends on the degree of water saturation  $S_w$  and WVDI. At a given  $S_w$  level, the  $D_{rc}$  is larger for a higher  $w/c$  ratio. The role of the  $w/c$  ratio in the  $D_{rc}$ - $S_w$  relation, however, becomes less pronounced with increasing  $w/c$  ratio. There exists a critical saturation, below which the water-filled capillary pores are discontinuous and the  $D_{rc}$ -value tends towards infinitely small. An increase of the  $w/c$  ratio results in a decrease of the critical saturation level.

**Keywords** Chloride diffusion · Mortar · Moisture distribution · Water saturation · Pore size distribution

## 1 Introduction

Chloride-induced corrosion is nowadays the main durability concern for the reinforced concrete structures in marine environment. Whenever the chloride concentration at the steel surface reaches a critical level, along with enough oxygen and moisture, steel corrosion may take place, resulting in cracking and spalling of the cover concrete and hence shortening the service life of the concrete structures [1].

Current durability design, e.g. DuraCrete [2], relies on the chloride diffusion coefficient of saturated concrete. In reality, however, concrete is often partially saturated. The interior relative humidity of

---

Y. Zhang (✉) · G. Ye  
Section of Materials and Environment, Department of  
3MD, Faculty of Civil Engineering and Geosciences,  
Delft University of Technology, Stevinweg 1,  
2628 CN Delft, The Netherlands  
e-mail: y.zhang-1@tudelft.nl

M. Zhang  
Advanced and Innovative Materials (AIM) Group,  
Department of Civil, Environmental and Geomatic  
Engineering, University College London, Gower Street,  
London WC1E 6BT, UK

concrete, as a result of self-desiccation, can be as low as 80% [3]. The concretes exposed to the atmospheric and tidal marine conditions undergo variations in moisture distribution with time. Even for an underwater concrete, splitting it longitudinally, only the outer few centimeters have a wet look while the interior part is rather dry [4]. The propagation of the saturation front in the concrete depends on the pore size and elapsed time after contact with water [5]. In the absence of sufficient knowledge about the effect of non-saturated state on chloride diffusion, the service life prediction based on the chloride diffusion coefficient of saturated concretes may give rise to misjudgement of the actual serviceability of reinforced concrete structures. In this regards a critical understanding of the non-saturated chloride diffusion is meaningful.

Chloride diffusion occurs only if water is present. In *saturated* concrete, the connected pores are responsible for the ionic transport. In *partially saturated* concrete, the connected water-filled pores provide the main pathways for the ionic transport. It is well known that the water phase is inclined to fill the small pores in the form of capillary condensed water, which allows for chloride diffusion. The gas phase, on the contrary, tends to fill the central region of the large pores and forms the gas phase clusters, which can block the passage of chloride diffusion [6]. The water content and its distribution in the pore structure are the key factors that influence the chloride diffusion in partially saturated concrete.

Since early in this century increasing attention has been given to study the chloride diffusion in non-saturated cementitious materials, yet up to date only a limited amount of experimental investigations can be found in the literature. These investigations were based on either direct diffusion tests or conductivity technique. For the direct diffusion tests, a chloride source can be imposed on the outer surface of unsaturated concretes through gaseous hydrogen chloride [7], chloride-containing solution [8] or solid crystal (sodium chloride) [9]. After a certain period of test, the chloride profiles were obtained by grinding successive parallel layers and quantifying the chloride content in each layer with potentiometric titration [10]. The Fick's 2nd law was then applied to quantify the non-saturated chloride diffusion with and without chloride binding considerations [7, 8]. It is worthwhile to note that imposing the different chloride sources

into unsaturated concretes may lead to unwanted moisture redistribution and/or microstructural alteration in the concretes. The conductivity technique, combined with the Nernst-Einstein equation, is an alternative approach to determine the chloride diffusion coefficient in the non-saturated cementitious materials [11–16]. Compared to direct diffusion tests, conductivity measurements are fast and easy to perform. Nevertheless, the conductivity technique is unable to consider the chloride binding effect.

So far the effect of non-saturated state on the chloride diffusion in cementitious materials remains a pending issue. The published results with respect to the relationship between chloride diffusion coefficient and moisture content show a large scatter [6]. The role of water-to-cement ( $w/c$ ) ratio in the non-saturated chloride diffusion is still a point of controversy in view of the existing research works [7, 13, 17]. The moisture distribution in the pore structure and its effect on the non-saturated chloride diffusion are not clear.

The present work aims to experimentally study the influence of moisture condition, including moisture content and its distribution, on the chloride diffusion in the partially saturated ordinary Portland cement mortar. The mortar samples with  $w/c$  ratios of 0.4, 0.5 and 0.6, cured for 1 year, are preconditioned in an oven at 50 °C to reach uniform water saturations ranging from 18 to 100%. The relative humidities of the mortar samples at different water saturation levels, i.e. water vapour desorption isotherm (WVDI), are measured. The effects of  $w/c$  ratio on the pore structure, measured from mercury intrusion porosimetry tests, and on the WVDI are analyzed. The conductivities of the partially saturated cement mortars and their pore solutions are derived based on experiments and, by using the Nernst-Einstein equation, the relative chloride diffusion coefficient  $D_{rc}$  is subsequently expressed as a function of the degree of water saturation  $S_w$ . Finally, the roles of the moisture distribution and the  $w/c$  ratio in the  $D_{rc}$ - $S_w$  relation are discussed in detail.

## 2 Experimental program

### 2.1 Materials and sample preparation

Ordinary Portland cement CEM I 42.5 N (OPC) was used to cast cement pastes and mortars. The mean



particle size, measured by laser diffraction, was 24.1  $\mu\text{m}$  for the cement powders.

The cement pastes were prepared for pore structure measurements. The cement powders and distilled water were mixed with a HOBART mixer at low speed for 1 min and at high speed for 2 min. The fresh pastes were poured into plastic bottles. The bottles were shaken continuously to remove air bubbles and sealed with lids thereafter. In order to avoid bleeding, the paste samples were rotated for 1 day before placing them in the curing room at  $20 \pm 0.1$  °C. After the age of 370 days, the hardened paste samples were taken out of the plastic bottles and crushed into small pieces (around 1  $\text{cm}^3$ ). The paste pieces were immersed in liquid nitrogen at  $-195$  °C for 5 min, and then placed in a freeze-dryer with  $-24$  °C and under vacuum at 0.1 Pa. Until the water loss was below 0.01% per day, the paste pieces can be ready for pore structure measurements.

The cement mortars were prepared for water vapour desorption tests and resistivity tests. The mortar samples were made with the same amount of siliceous sand (according to EN 196-1), but with different  $w/c$  ratios of 0.4, 0.5 and 0.6. The particle size of the siliceous sand was in the range of 0.125–2 mm. The cement binder to sand ratio was 1:3 by weight. Cylindrical mortars ( $\phi 100 \times 80$  mm) were cast. After wet-cured at  $20 \pm 0.1$  °C for 370 days, the top and bottom surfaces of the mortar samples with thickness of 15 mm were cut off. The middle part of each mortar sample was stored in lime water for 1 week, followed by the sample preconditioning procedures as will be described in Sect. 2.2.

For the sake of description, the paste samples with  $w/c$  ratios of 0.4, 0.5 and 0.6 are abbreviated as P4, P5 and P6, respectively; the mortar samples with  $w/c$  ratios of 0.4, 0.5 and 0.6 are abbreviated as M4, M5 and M6, respectively.

## 2.2 Sample preconditioning for desired moisture content

At present, “RH” (relative humidity) preconditioning and “SD” (saturation degree) preconditioning are the main approaches for preparing partially saturated cementitious samples [6]. In both approaches the samples are usually wet-cured until a high maturity, followed by a series of drying procedures to reach desired moisture contents. For “RH” preconditioning,

the sample (often saturated) is dried step-by-step under drier humidity circumstances until the sample is in equilibrium to the target humidity level, i.e. water loss  $< 0.02$  g/week [13]. The different humidity circumstances can be controlled by saturated salt solutions [18]. For “SD” preconditioning, the sample (often saturated) is firstly dried in an oven at a relatively high temperature to get a preassigned loss of water and then conducted with a moisture redistribution step in order to gain homogeneous moisture distribution [19].

The two approaches were evaluated at the beginning of the sample preconditioning. The “RH” preconditioning approach was found to be time-consuming, and it was difficult to reach the equilibrium moisture contents for the low humidity circumstances because of the low moisture diffusivity of the samples. The “SD” preconditioning approach, on the contrary, was convenient and fast. In the present work, all mortar samples with desired moisture contents were obtained from the “SD” preconditioning approach.

Degree of water saturation,  $S_w$ , was used to quantify the moisture content of the mortar samples. The  $S_w$ -value is defined as the ratio of the volume of pore water over the total pore volume in the sample, as shown in Eq. (1a). The water absorption,  $A_b$ , is expressed in Eq. (1b).

$$S_w = \frac{m_h - m_d}{m_s - m_d} \quad (1a)$$

$$A_b = \frac{m_s - m_d}{m_d} \quad (1b)$$

where  $m_h$  [g] is the mass of the sample at a particular saturation state,  $m_s$  [g] is the mass of the sample at saturated state and  $m_d$  [g] is the mass of the dried sample. The parameters  $A_b$ ,  $m_s$ ,  $m_d$  and  $m_h$  were all determined by following the procedures described in Ref. [19].

The sample mass,  $m_h$ , corresponding to a particular saturation  $S_w$  level can be deduced from Eq. (1a–1b).

$$m_h = m_s \frac{1 + A_b \cdot S_w}{1 + A_b} \quad (2)$$

The sample preconditioning of the present work, which was similar to that used in Ref. [19], proceeded with three steps. The details will be described in the following.



*Step one: drying each sample at 50 °C to reach its desired  $S_w$ -value*

1. The lateral and bottom sides of the mortar sample (50-mm thick) were sealed with electric isolating tape to avoid any multi-directional moisture transfer. Only the top side of the sample was left as the drying surface.
2. The mortar sample was moved into a ventilated oven, which was heated gradually at a rate of 5 °C per hour up to 50 °C. A CO<sub>2</sub> absorbent (sodium hydroxide) was placed in the oven to minimize the carbonation effect.
3. The oven was vacuumed until the pressure was below 50 Pa. The low pressure circumstance enables to dry the sample to a low  $S_w$  level in a relatively short period.
4. The mass loss was recorded at frequent intervals during the first 6 h, followed by one measurement per day later on.

*Step two: monitoring moisture homogeneity by a moisture redistribution procedure*

Once the sample mass  $m_h$  corresponding to a particular saturation  $S_w$  level reaches its desired value, there may still be a moisture gradient from the bottom to the top of the mortar sample. A moisture redistribution procedure is required so far as the homogeneous moisture distribution is concerned. To this end, all the surfaces (top, bottom and lateral) of the sample were tightly sealed with isolating tape. The sample was then stored in a plastic bag at 50 °C for a certain period, i.e. 7–45 days, depending on the saturation  $S_w$  level of the sample. The storage period was longer for the sample with a lower  $S_w$  level. At this stage, a great deal of moisture was transferred from the bottom to the top of the sample. Next, the sample was gradually

cooled down to  $30 \pm 0.1$  °C. A novel set-up shown in Fig. 1 was established to monitor the moisture homogeneity by measuring the RH of both surfaces (top and bottom) of the sample. A similar method for monitoring the moisture homogeneity of cylindrical samples has been previously used in Ref. [20].

1. The isolating tape on the top and bottom surfaces of the mortar sample was removed. The lateral surface of the mortar sample was still sealed.
2. The mortar sample was placed in a cylindrical chamber. The chamber was sealed with lid and maintained a constant temperature of  $30 \pm 0.1$  °C. The time-related RH changes at the top and bottom surfaces of the sample were monitored with the same type of hygrometer. As expected, the RH-value on the top surface was increasing while that on the bottom surface was decreasing. Once the RH-values on both surfaces approached the same value (difference less than 1%), the moisture distribution inside the sample was considered homogeneous.
3. The sample was cooled down slowly with 5 °C per hour to room temperature ( $20 \pm 0.1$  °C).
4. The sample was removed from the chamber. All the surfaces (top, bottom and lateral) of the sample were tightly sealed with isolating tape. The sample was then stored in a plastic bag to keep its specific water saturation level.

*Step three: evaluation on the preconditioned samples*

An evaluation step was performed on the preconditioned samples in order to check the efficiency of the preconditioning approach introduced in this work.

Firstly, drying at 50 °C may influence the phase mineralogy and the pore structure of the mortar sample

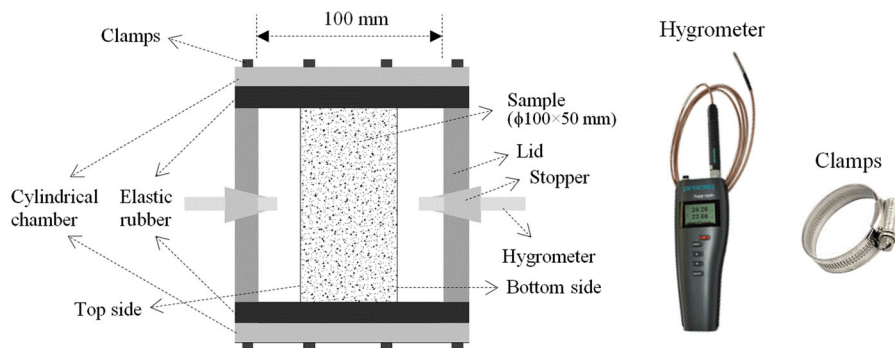


**Fig. 1** Set-up for monitoring the moisture homogeneity of mortar sample ( $\phi 100 \times 50$  mm)



and, therefore, can affect the calculated water saturation level of the sample when Eq. (2) is applied for the calculation. The details will be given in Sect. 4.1 in this respect.

Secondly, the preconditioned mortar samples were examined under an optical microscope ( $\times 100$ ). No micro-cracking was observed in this magnification. The possibility of crack initiation was minimized due to two reasons: (a) no large moisture or temperature gradient occurred at any time of a series of preconditioning procedures; (b) the moisture moved towards only one direction in the whole sample preconditioning process.

All mortar samples, preconditioned with desired water saturation levels, were ready for the resistivity measurements. The details will be given in Sect. 2.5.2.

### 2.3 Pore structure of cement paste

In partially saturated pore systems the ionic diffusion primarily depends on the water-filled pores. The water-filled pores are usually small. A deep insight into the pore structure, especially the structure of the small capillary pores, becomes a prerequisite for capturing the non-saturated ionic diffusion.

Mercury intrusion porosimetry (MIP) is a technique commonly used to characterize the pore structure of cementitious materials [21]. It is known that the 1st intrusion of MIP test, due to the ink-bottle effect, is considered inappropriate to identify the real pore size distribution [22]. The 2nd intrusion, however, has little ink-bottle effect and provides a more truthful size distribution of the small capillary pores in cement paste [23].

An example of the cumulative intrusion volume with applied pressure is shown in Fig. 2, in which the extrusion curves in the 1st and 2nd cycles are almost overlapped. It is clear that the 1st intrusion-extrusion cycle shows a serious ink-bottle effect, as indicated by the ink-bottle porosity, but there is little ink-bottle effect in the 2nd intrusion-extrusion cycle. In this work, the 2nd intrusion was applied to characterize the pore size distribution of the cement pastes with various  $w/c$  ratios.

The relationship between pore diameter  $d$  [ $\mu\text{m}$ ] and applied pressure  $P$  [MPa] is determined by the Washburn equation [24]:

$$d = -\frac{4\gamma_{\text{Hg}} \cos \theta_m}{P} \quad (3)$$

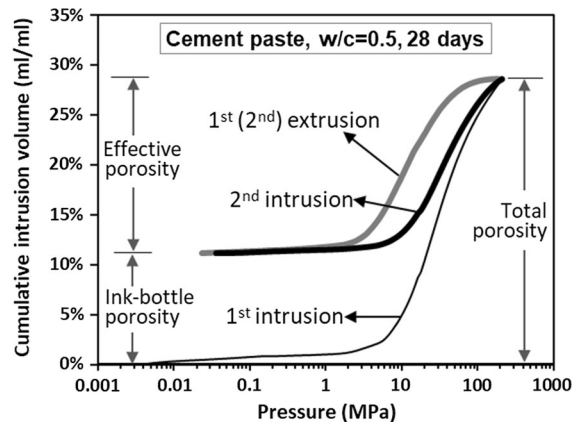


**Fig. 2** An example of the cumulative intrusion volume obtained from MIP in the 1st and 2nd intrusion-extrusion cycles

where  $\gamma_{\text{Hg}}$  is the surface tension of mercury (0.48 kN/m);  $\theta_m$  is the contact angle between mercury and cement paste ( $139^\circ$  for mercury intrusion).

Pore connectivity is a key parameter that influences the transport properties of cementitious materials. It is often expressed as the ratio between the volume of the continuous pores and the total pore volume. The pore connectivity  $\eta_p$  can be deduced from the MIP test [25], and calculated as the quotient of the effective porosity  $\phi_e$  over the total porosity  $\phi_t$ .

$$\eta_p = \frac{\phi_e}{\phi_t} \times 100\% \quad (4)$$

### 2.4 Water vapour desorption isotherm of cement mortar

Water vapour desorption isotherm (WVDI) illustrates the changes of the interior relative humidity RH with different degrees of water saturation  $S_w$ . According to the Kelvin law, each RH level corresponds to a particular pore diameter. Below this diameter all the pores are considered filled with water. These water-filled pores constitute a major contribution to the ionic transport. The relationship between WVDI (RH vs.  $S_w$ ) and pore structure will be analyzed based on the Kelvin law in order to examine the moisture distribution and ionic transport in the non-saturated cement mortars.



### 2.4.1 RH– $S_w$ relationship

The RH of the mortar sample at a particular saturation  $S_w$  level was recorded when the sample exhibited homogenous moisture distribution at  $20 \pm 0.1$  °C, as illustrated in Fig. 1. The water vapour desorption isotherms (RH vs.  $S_w$ ) in the cement mortars with  $w/c$  ratios of 0.4, 0.5 and 0.6 were determined.

This RH– $S_w$  relationship is not valid, in theory, for the very surface-near parts of the specimens since they have been dried and rewetted. Those parts follow instead a scanning-curve. The effect of this should, however, be minor since the surfaces are somewhat wetted when a wet sponge is applied when the conductivity measurements are done.

### 2.4.2 Evaluation of moisture distribution

The interior RH of cementitious material is mainly associated with the meniscus formed above the water-filled pores. The Kelvin equation [26] gives:

$$\ln(\text{RH}) = -\frac{2\gamma_w V_m \cos \theta_w}{r_k RT} \quad (5)$$

where  $\gamma_w$  is the surface tension of water (0.072 N/m in pure water);  $V_m$  is the molar volume of water [ $\text{m}^3/\text{mol}$ ];  $\theta_w$  [°] is the contact angle between water and solids (it is assumed to be zero for water);  $R$  is the ideal gas constant (8.314 J/mol K);  $T$  is the absolute temperature [K];  $r_k$  is the meniscus radius [m]. The Kelvin equation is able to provide a valid estimation for the menisci with radius  $r_k$  as low as 4 nm, with a discrepancy of  $\pm 6\%$  when the radius is within 4–20 nm [27].

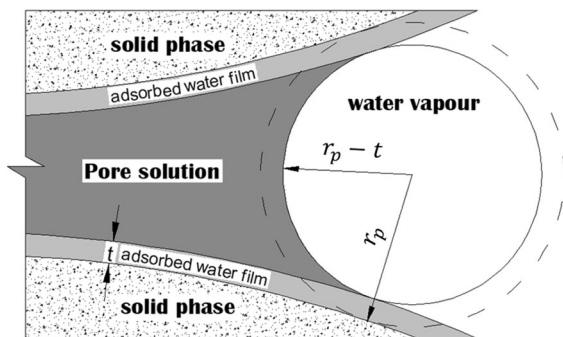


**Fig. 3** Meniscus curvature and adsorbed water film in the capillary pores



If the adsorbed water film is taken into account, as illustrated in Fig. 3, the Kelvin equation is replaced by the Kelvin–Cohan equation [28], as:

$$\ln(\text{RH}) = -\frac{2\gamma_w V_m \cos \theta_w}{(r_p - t)RT} \quad (6)$$

where  $r_p$  is the radius [m] of the pores in which the meniscus surface is formed.  $d_p$  ( $d_p = 2r_p$ ) is considered as the *smallest drained pore diameter* in a partially saturated specimen; herein, a pore is defined as drained when the pore is only covered with the nano-scale water film.  $t$  [m] is the thickness of the water film, which is a function of the interior RH [29]:

$$t = [0.385 - 0.189 \cdot \ln(-\ln(\text{RH}))] \times 10^{-9} \quad (1\% \leq \text{RH} \leq 95\%) \quad (7)$$

## 2.5 Conductivity of cement mortar at different water saturations

### 2.5.1 Diffusion coefficient and conductivity: Nernst–Einstein equation

When a cementitious material is considered a solid electrolyte, the chloride diffusion coefficient of the cementitious material can be related to its electrical conductivity [30, 31]. Cementitious material is a three-phase system consisting of pore solution phase, solid phase and vapour phase. The conductivity of the pore solution phase is usually many orders of magnitude higher than that of the solid phase and vapour phase [32]. The Nernst–Einstein equation shows that the ratio of conductivity  $\sigma_0$  [S/m] of the pore solution to conductivity  $\sigma$  of the cementitious material is equal to the ratio of chloride diffusion coefficient  $D_0$  [ $\text{m}^2/\text{s}$ ] in the pore solution to chloride diffusion coefficient  $D$  in the cementitious material.

$$\frac{\sigma_0}{\sigma} = \frac{D_0}{D} \quad (8)$$

The coefficient  $D_0$  is around  $1.5 \times 10^{-9}$   $\text{m}^2/\text{s}$  at room temperature when the chloride concentration is within 0.1–1.0 mol/l [33]. The  $\sigma_0$ -value relies on the pore solution chemistry. The conductivity  $\sigma$  of cementitious material is the inverse of its resistivity  $\rho_e$  [ $\Omega\text{m}$ ], which is a function of the electrical resistance  $R_{\text{mat}}$  of the material, as:

$$\sigma = \frac{1}{\rho_e} = \frac{mL}{A} \cdot \frac{1}{R_{\text{mat}}} \quad (9)$$

where  $m$  is the geometry factor ( $m = 1$  for cylindrical specimen);  $L$  [m] is the length of the specimen;  $A$  [m<sup>2</sup>] is the cross sectional area of the specimen.

### 2.5.2 Resistivity measurement of cement mortar

Figure 4 shows the experimental set-up for resistivity measurement (under direct current) on a partially saturated mortar specimen. For the principles of the resistivity measurement reference is made to Polder [34]. In the present work the resistivity measurements were performed at room temperature ( $20 \pm 0.1$  °C). The top and bottom sides of the specimen were exposed as the measuring surfaces, with the lateral side sealed. The electrical resistance  $R_{\text{mat}}$  of the specimen ( $\phi 100 \times 50$  mm) was measured with one stainless steel electrode covering each end of the specimen. A wet sponge was applied between specimen surface and each electrode to ensure the whole surface specimen under current flow. During the test, the measured resistance  $R_{\text{mat}}$  was found to decrease with time. This was caused by the moisture transfer from the wet sponge into the specimen. To minimize this effect, the result obtained from the first measurement was adopted. The adoption of the first measurement was based on two considerations. *First*, the top, middle and bottom parts of the specimen can exhibit almost the same moisture level when the whole specimen was tightly sealed with isolating tape. After the isolating tape on the top and bottom surfaces of the specimen was removed, wetting the surface specimen by using the wet sponge was considered an instantaneous process. *Second*, the measured  $R_{\text{mat}}$  value showed a gradually decreasing trend with time. If wetting the surface specimen with the wet sponge was not an instantaneous process, an abruptly sharp drop of

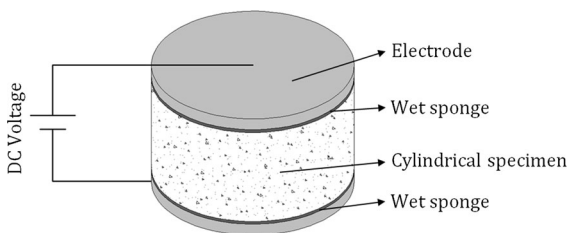


**Fig. 4** Resistivity measurement on a cylindrical specimen under direct current (DC)

the  $R_{\text{mat}}$  value will occur in a few seconds after the first measurement. However, such abruptly sharp drop was not found in the present study.

Each specimen has been weighed before and after the resistivity test. The weight increase of each tested specimen was less than 0.2 g, due to the use of wet sponge, which led to a change of the water saturation  $S_w$  inside the specimen of around 0.2%. This minor amount was negligible.

### 2.5.3 Relative chloride diffusion coefficient of cement mortar

Based on the resistivity measurements, and using Eqs. (8) and (9), the chloride diffusion coefficients of the cement mortars at various water saturations were obtained. Relative chloride diffusion coefficient ( $D_{\text{rc}}$ ) is expressed as the *ratio* of chloride diffusion coefficient at a particular saturation  $S_w$  level ( $D_{S_w}$ ) to that at saturated state ( $D_{\text{Sat}}$ ), as:

$$D_{\text{rc}} = \frac{D_{S_w}}{D_{\text{Sat}}} = \frac{\sigma_{S_w}}{\sigma_{\text{Sat}}} \cdot \frac{\sigma_{0,\text{Sat}}}{\sigma_{0,S_w}} \quad (10)$$

For each mortar mixture,  $\sigma_{S_w}$  and  $\sigma_{\text{Sat}}$  are the conductivities of cement mortar at a particular saturation  $S_w$  and at saturated state, respectively. The both can be obtained directly from the resistivity tests.  $\sigma_{0,S_w}$  and  $\sigma_{0,\text{Sat}}$  are the conductivities of pore solutions when the cement mortar is at a particular saturation  $S_w$  and at saturated state, respectively. The determination of  $\sigma_{0,S_w}$  and  $\sigma_{0,\text{Sat}}$  is rather complex, which will be discussed in detail in Sect. 4.2.

## 3 Experimental results

### 3.1 Pore size distribution of cement pastes

The pore structures of the 1-year-old cement pastes were measured by the MIP tests. As introduced in Sect. 2.3, each MIP test consisted of a 1st intrusion and a 2nd intrusion. Figure 5a shows the results of the differential pore size distribution (PSD) obtained from the 1st intrusion. These PSD curves exhibit intersections, and it is not easy to identify the role of the  $w/c$  ratio in the truthful size distribution of the small pores (<200 nm). This can be ascribed to the presence of ink-bottle pores, whose volumes have been



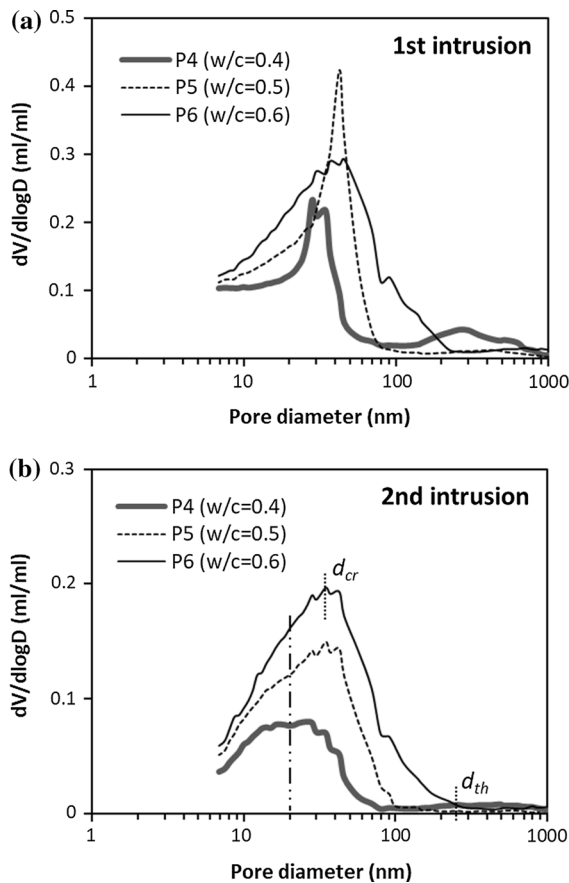


**Fig. 5** Differential pore size distributions of the 1-year-old cement pastes: **a** from the 1st intrusion of MIP; **b** from the 2nd intrusion of MIP;  $d_{cr}$  and  $d_{th}$  are marked for the cement paste P6 as critical diameter and threshold diameter, respectively

included in the PSD results obtained from the 1st intrusion.

Figure 5b shows the PSD curves obtained from the 2nd intrusion. Since the volumes of ink-bottle pores are excluded, the role of the  $w/c$  ratio in the small pore sizes can be revealed more clearly. Each curve shows a main peak. The pore diameters corresponding to the top and the onset of the main peak are defined as critical diameter  $d_{cr}$  and threshold diameter  $d_{th}$ , respectively. In the cement pastes P4, P5 and P6, the  $d_{cr}$ -values are determined as 26.2 nm, 34.6 nm and 34.6 nm, and the  $d_{th}$ -values are 79.5, 112.6 and 225.7 nm, respectively. Obviously, the  $w/c$  ratio greatly alters the capillary pore size range from  $d_{cr}$  to  $d_{th}$ . The PSD curves of pastes P5 and P6 are more close to each other (especially for the pores < 20 nm),

but they are very different from the PSD curve of paste P4 in both size and shape.

### 3.2 Water vapour desorption isotherm of cement mortars

Figure 6 shows the water vapour desorption isotherms in the cement mortars with  $w/c$  ratios of 0.4, 0.5 and 0.6. In general, the interior RH decreases with decreasing water saturation  $S_w$  level. The RH decrease, however, is much less pronounced in the cement mortar with a higher  $w/c$  ratio. Take mortar M6 ( $w/c = 0.6$ ) for an example, a significant decrease of the  $S_w$  from 95 to 65% results in a small decrease of the RH from 98 to 90%. In contrast, a much larger decrease of the RH from 98 to 70% is observed for mortar M4 ( $w/c = 0.4$ ) when the  $S_w$  decreases in the same range. It is worth noting that in the range of 50–90% RH, corresponding to the smallest drained pore diameter  $d_p$  of 4.0–21.8 nm, almost linear RH– $S_w$  patterns can be observed for all the  $w/c$  ratios, but that these linear relationships vary with different  $w/c$  ratios. For a given water saturation an increase of the  $w/c$  ratio results in an increase of the RH. This agrees with previous results from Parrott [35]. The RH– $S_w$  curves for M5 and M6 are closer, compared to that of M4. For instance, at RH = 60%, the  $S_w$ -values are 54, 31 and 27% for the mortars M4, M5 and M6, respectively.

The interior RH is primarily controlled by the meniscus formed above the water-filled pores. With decreasing water saturation  $S_w$ , the water loss occurs

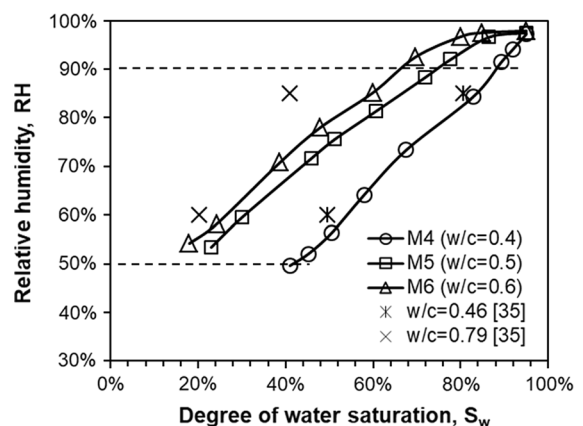


**Fig. 6** Water vapour desorption isotherms in the 1-year-old cement mortars with varying  $w/c$  ratios

preferably from large pores to small pores. The specimen with a higher  $w/c$  ratio, e.g. M6, contains more large pores and thus can maintain a high interior RH even at a relatively low  $S_w$  level. In contrast, for the specimen with a lower  $w/c$  ratio (e.g. M4), the interior RH is more sensitive to the water content and the RH-value falls off rapidly as soon as the  $S_w$  starts to decrease from saturated state. The closer RH- $S_w$  curves for mortars M5 and M6, as shown in Fig. 6, are attributable to the similar pore structures of their paste matrixes, as already described in Sect. 3.1.

### 3.3 Relative chloride diffusion coefficient of cement mortars

Based on Eq. (10), the relative chloride diffusion coefficient  $D_{rc}$  was expressed as a function of the degree of water saturation  $S_w$ . It should be mentioned that at very low saturation levels the conductivities of the mortar specimens were infinitely small. In these specimens the water-filled capillary pores were assumed discontinuous. The term *critical saturation* is introduced to describe the water saturation level, below which the water-filled capillary pores are unable to form a continuous path for ionic diffusion.

Figure 7 shows the  $D_{rc}$ - $S_w$  relations in the cement mortars with various  $w/c$  ratios. In general, the  $D_{rc}$ -value decreases with decreasing  $S_w$ . The  $D_{rc}$ - $S_w$  relation can be divided into three stages. Take mortar M6 as an example, when the  $S_w$  decreases from saturated state, the  $D_{rc}$ -value shows a slight decrease

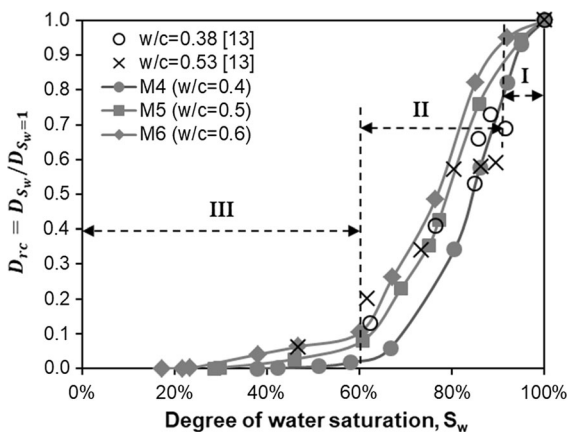


**Fig. 7** Relative chloride diffusion coefficient  $D_{rc}$  as a function of water saturation  $S_w$  in the 1-year-old cement mortars with varying  $w/c$  ratios

(stage I). There is a sharp drop in the  $D_{rc}$ -value when the  $S_w$  reduces from 90 to 60% (stage II), followed by a slight decline (stage III). An increase of the  $w/c$  ratio results in an increase of the  $D_{rc}$ -value. For example, at  $S_w = 80\%$ , the  $D_{rc}$ -value is 0.34 for mortar M4, compared to  $D_{rc} = 0.58$  and  $D_{rc} = 0.67$  for mortars M5 and M6, respectively. The  $D_{rc}$ - $S_w$  curves for M5 and M6 are closer compared to that for M4. It indicates that the role of the  $w/c$  ratio in the  $D_{rc}$ - $S_w$  relation becomes less pronounced with increasing  $w/c$  ratio. The same finding has been reported in a previous simulation work as presented in [17].

Once the water saturation  $S_w$  is lower than the critical saturation  $S_{cr}$  level, the  $D_{rc}$ -value tends towards infinitely small. In this work the critical saturation  $S_{cr}$  of each mortar was estimated based on the changes of the electrical resistance  $R_{mat}$  when the water saturation  $S_w$  decreases in the stage III. An example for determining the critical saturation  $S_{cr}$  is given in Fig. 8, where the plots ( $R_{mat}$  vs.  $S_w$ ) for mortar M6 are presented. To better assess the relationship ( $R_{mat}$  vs.  $S_w$ ), schematic representations of the moisture distribution in the cementitious system at water saturation  $S_w$  above/below the critical saturation  $S_{cr}$  are inserted in Fig. 8. There are capillary pores (diameters  $d_1 > d_2$ ) and interlayer (gel) pores in the porous system.

- At  $S_{cr} < S_w \leq 60\%$ , the capillary pores  $d_1$  are partially water-filled, and the capillary pores  $d_2$  are

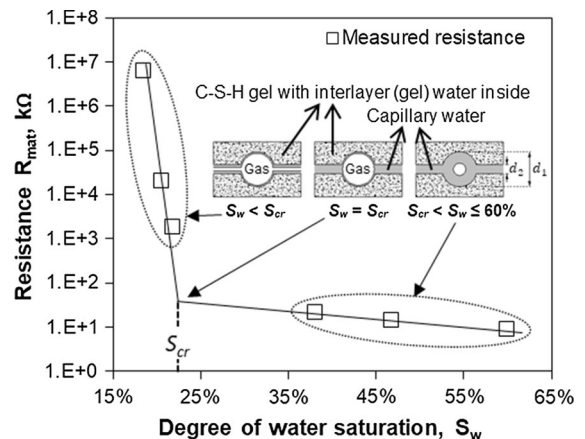


**Fig. 8** Moisture distribution and electrical resistance  $R_{mat}$  at water saturation  $S_w$  levels above/below the critical saturation  $S_{cr}$ . The resistances  $R_{mat}$  were measured from resistivity tests performed on the mortar specimens (M6:  $w/c = 0.6$ , size  $\phi$  100 × 50 mm) at low saturation levels ( $S_w = 18$ –60%)

fully water-filled. The capillary water can form a continuous path that dominates the ion conduction/diffusion in the system. A decrease of the  $S_w$  level results in an increase of the resistance  $R_{\text{mat}}$ .

- At  $S_w = S_{\text{cr}}$ , the capillary pores  $d_1$  are drained (only thin water film is present). The fully water-filled capillary pores  $d_2$  become discontinuous. In this case, the interlayer (gel) water in the C–S–H gel is responsible for the ion conduction/diffusion. The resistance  $R_{\text{mat}}$  is very high, and the ionic diffusion coefficient is infinitely small.
- At  $S_w < S_{\text{cr}}$ , the capillary pores  $d_1$  are drained, and the capillary pores  $d_2$  become partially water-filled. The interlayer (gel) water in the C–S–H gel dominates the ion conduction/diffusion. The resistance  $R_{\text{mat}}$  is much higher than that in the case of  $S_w > S_{\text{cr}}$ . In addition, the increase of the resistance  $R_{\text{mat}}$  with decreasing  $S_w$  is more pronounced, compared to that in the case of  $S_w > S_{\text{cr}}$ .

As indicated in Fig. 8, the increase of the resistance  $R_{\text{mat}}$  with decreasing  $S_w$  can be categorized into two groups according to the  $S_w$  above or below the critical saturation  $S_{\text{cr}}$ . Each group tends to present an approximately linear relationship ( $R_{\text{mat}}$  vs.  $S_w$ ). The  $S_w$  level corresponding to the intersection of the two lines is estimated as the critical saturation  $S_{\text{cr}}$ . On this basis, the critical saturations  $S_{\text{cr}}$  are found to be approximately 37, 28 and 22% for the cement mortars with  $w/c$  ratios of 0.4, 0.5 and 0.6, respectively. The accuracy of the obtained  $S_{\text{cr}}$ -values is expected to be higher in the case when more specimens at low saturation levels ( $S_w = 18\text{--}60\%$ ) were prepared for the resistivity measurements.

## 4 Discussion

### 4.1 Influence of sample preconditioning on the microstructure of cementitious samples

In order to obtain desired saturation levels, in this study the samples were pre-treated by drying in an oven. This process is a quick method to obtain cementitious samples with less water content. However, oven-drying at a relatively high temperature and the resultant declining RH can affect the thermodynamic stability of the hydration products. As a result,

the porosity and associated water saturation  $S_w$  inside the preconditioned samples may be influenced.

#### 4.1.1 Effect of temperature on microstructure

The hydration products show different sensitivities to the exposure temperature. Calcium hydroxide (CH) is relatively stable, which decomposes at a temperature higher than 440 °C [36]. The decomposition temperature of the main hydrates, i.e. calcium-silicate-hydrate (C–S–H), is not well established, but it is considered that C–S–H may lose a considerable amount of non-evaporable water at 105 °C [37]. Crack initiation has also been reported at this temperature [38]. The AFm phases, i.e. a family of hydrated calcium aluminates, can be decomposed in a wide range of temperature, i.e. 75–250 °C [39]. The dehydration of gypsum starts at approximately 80 °C [40]. The decomposition of ettringite (AFt) commences at around 60 °C [41].

It is evident that drying at elevated temperatures makes the water loss faster but may result in more severe microstructural alterations. For the hardened cement paste oven-dried at 50 °C after 4 weeks, the pores larger than 8 nm were found to be increased and the pores smaller than 8 nm decreased, while the total pore volume remained unchanged [42]. 50 °C is recommended as the most efficient drying temperature for cementitious materials, because it costs the least time meanwhile the minimum microstructural alterations [43]. Given all these aspects, 50 °C was selected for the oven drying temperature in this work.

#### 4.1.2 Effect of relative humidity on microstructure

The change of interior RH influences various hydrates to different extents. At 25 °C, the monosulfoaluminate (Ms) starts to dehydrate at RH = 97%; its volume is reduced by 8% at RH = 50%, and by 15% when the RH is as low as 8% [44]. Hydroxy-AFm is found until RH = 97%, and it is completely dehydrated from OH19-AFm into OH13-AFm at RH = 83%, and further into OH11-AFm at RH < 23%. The volume of the hydroxy-AFm decreases by around 27% when the interior RH reduces from 97 to 50% [44]. In contrast, the carboaluminate is stable along a wide range of exposure RH conditions (25–97% RH). The AFt phase is very robust against the interior RH, and



only one water molecule is lost when the RH drops from 97 to 8% [44].

#### 4.1.3 Evaluation on the change of porosity

The mortar samples were made with a constant cement binder-to-sand ratio (1:3 by weight). The specific gravity was  $3.12 \times 10^3 \text{ kg/m}^3$  for the cement and  $2.65 \times 10^3 \text{ kg/m}^3$  for the sand. Taking the mortar sample M5 as an example, the volume ratio of the paste matrix over the mortar was estimated as 32.58%. The interior RH of all the preconditioned samples was above 50%, which primarily resulted in the volume of the AFm phases (Ms and OH-AFm) reducing by 8–27%. With the assumption that the solid AFm phases constitute 15% by volume of the paste matrix [45], the interior RH reducing from 100 to 50% would result in the change of porosity of the sample M5 by  $15\% \times 32.58\% \times (8-27)\% = (0.39-1.32)\%$ . This minor porosity change, which has little influence on the water saturation level of the preconditioned sample, was not taken into account in this study.

#### 4.2 Conductivity of pore solution at various saturations

The chloride diffusion coefficients of cement mortars at various water saturations were calculated by using the Nernst–Einstein equation, where the conductivities of the pore solutions, viz.  $\sigma_0$ -values, have to be determined. According to Snyder et al. [46], the  $\sigma_0$ -value is mainly determined by the concentrations of ions, viz. hydroxide ( $\text{OH}^-$ ) and alkalis ( $\text{Na}^+$ ,  $\text{K}^+$ ), in the pore solution.

##### 4.2.1 Ionic concentrations at various saturations

For the cement mortars with  $w/c$  ratios of 0.4, 0.5 and 0.6, the pore solutions at  $S_w = 100\%$  were squeezed out from the 1-year cured saturated mortar specimens. The concentrations of the alkalis ( $\text{Na}^+$ ,  $\text{K}^+$ ) in these pore solutions were measured by means of inductively coupled plasma optical emission spectrometry (ICP-OES). The concentration of  $\text{OH}^-$  was considered as equal as the sum of alkalis ( $\text{Na}^+$ ,  $\text{K}^+$ ) concentrations [47].

In principle, the alkalis ( $\text{Na}^+$ ,  $\text{K}^+$ ) released during cement hydration are either bound by hydrates (mainly C–S–H) or freely present in the pore solution [47]. The

relationship between bound and free alkalis is dependent on the mass of C–S–H [48]. At a particular saturation ( $S_w < 100\%$ ), the concentrations of the alkalis ( $\text{Na}^+$ ,  $\text{K}^+$ ) can be predicted according to the method developed by Chen and Brouwers [48]:

$$C_{\text{Na}} = \frac{n_{\text{Na}}^r}{V_w + Rd \cdot m_{\text{C-S-H}}} \quad (11)$$

$$C_{\text{K}} \cdot V_w + K_f \cdot (C_{\text{K}})^{0.24} \cdot m_{\text{C-S-H}} = n_{\text{K}}^r \quad (12)$$

Various parameters are described as follows:

- Rd is the distribution ratio ( $Rd = 0.45 \times 10^{-3} \text{ L/g}$ );  $K_f$  is the adsorption coefficient ( $K_f = 0.20 \times 10^{-3} \text{ L/g}$ );  $V_w$  is the volume (L) of the pore solution, which depends on the total porosity and water saturation level of the specimen. The  $V_w$ -value was determined as 0.0726 L for the mortar specimen M4 ( $\phi 100 \times 50 \text{ mm}$ ) at  $S_w = 100\%$ .
- $m_{\text{C-S-H}}$  is the mass of C–S–H, which is simplified as the composition of  $\text{C}_{1.7}\text{SH}_4$  in the OPC mortars. The value of  $m_{\text{C-S-H}}$  was estimated by Thermogravimetric analysis (TGA/DSC) with the assumption that the released water was from the thermal decomposition of C–S–H (105–1100 °C) and CH (400–550 °C) [49]. For the mortar specimen M4,  $m_{\text{C-S-H}}$  was calculated as 100.67 g.
- $C_{\text{Na}}$  and  $C_{\text{K}}$  represent the concentrations (mol/L) of alkalis  $\text{Na}^+$  and  $\text{K}^+$ , respectively. From the ICP-OES tests,  $C_{\text{Na}}$  and  $C_{\text{K}}$  for the mortar specimen M4 at  $S_w = 100\%$  were determined as 0.176 and 0.341 mol/L, respectively.
- $n_{\text{Na}}^r$  and  $n_{\text{K}}^r$  refer to the moles of the alkalis, viz.  $\text{Na}^+$  and  $\text{K}^+$ , released during cement hydration. Substituting the values of the parameters ( $V_w$ ,  $m_{\text{C-S-H}}$ ,  $Rd$ ,  $C_{\text{Na}}$  and  $C_{\text{K}}$ ) at  $S_w = 100\%$  into Eqs. (11) and (12) allows for determining the values of  $n_{\text{Na}}^r$  and  $n_{\text{K}}^r$ , which were equal to  $n_{\text{Na}}^r = 0.0207 \text{ mol}$  and  $n_{\text{K}}^r = 0.0403 \text{ mol}$  for the mortar specimen M4.

In Eqs. (11) and (12), the parameters ( $n_{\text{Na}}^r$ ,  $n_{\text{K}}^r$ ,  $Rd$ ,  $K_f$  and  $m_{\text{C-S-H}}$ ) are considered to be independent of the water saturation  $S_w$  level except the  $V_w$ -value that is linearly proportional to the  $S_w$  level. On this basis, the alkalis concentrations ( $C_{\text{Na}}$  and  $C_{\text{K}}$ ) can be determined as a function of the  $S_w$  level.

#### 4.2.2 $\sigma_0$ -values at various saturations

Synthetic solutions were prepared by mixing the solids (NaOH, KOH) with distilled water in proper proportions in accordance to  $C_{Na}$  and  $C_K$  at each water saturation level. The conductivities of the pore solution at various saturations, viz.  $\sigma_0$ -values, were obtained through the conductivity measurements performed on these synthetic solutions. Figure 9a presents an example of the calculated ionic concentrations in the mortar M4. Figure 9b shows the measured  $\sigma_0$ -values in the mortars M4, M5 and M6. The conductivity of pore solution,  $\sigma_0$ , is almost two times larger when the water saturation decreases from 100 to 30%.

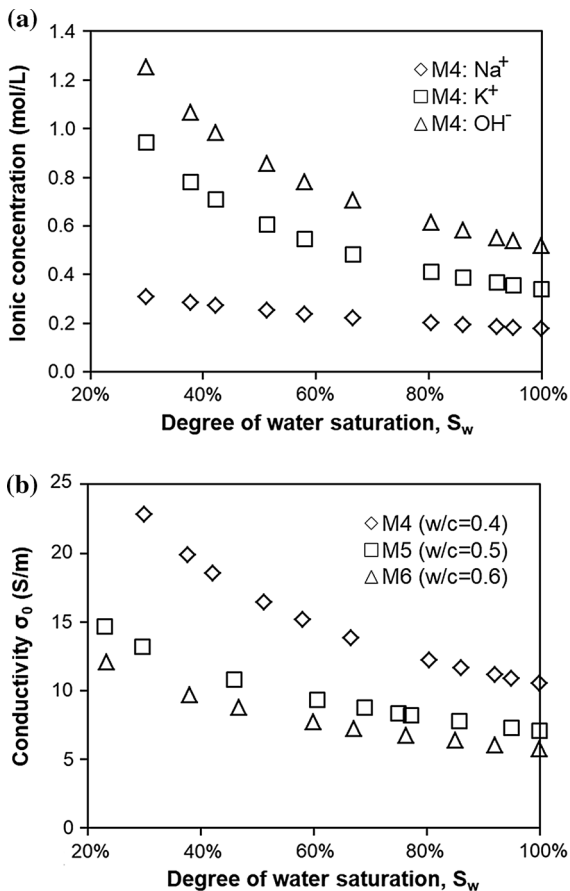


**Fig. 9** a Ionic concentration as a function of water saturation level in the cement mortar M4 (1 year old,  $w/c = 0.4$ ); b Conductivity  $\sigma_0$  of pore solution as a function of water saturation level in the cement mortars (1 year old) with  $w/c$  ratios of 0.4, 0.5 and 0.6

#### 4.3 Moisture distribution in partially saturated cement mortars

Figure 6 showed that the interior RH strongly depends on the water saturation  $S_w$ . At a particular RH, there is a smallest drained pore diameter  $d_p$  ( $d_p = 2r_p$ ) by following Eq. (6). The pores below the diameter  $d_p$  are filled with water allowing for ionic transport. The  $d_p$ - $S_w$  plots are used to describe the moisture distribution in the non-saturated cement mortars.

Based on the  $d_p$ -RH relation, the RH- $S_w$  plots (Fig. 6) were transformed into the  $d_p$ - $S_w$  plots, as presented in Fig. 10. With a decrease of water saturation  $S_w$  the  $d_p$ -value shows three-stage change, especially for the specimen at a high  $w/c$  ratio, viz. M6. The  $d_p$ -value falls off significantly in the high saturation range (e.g.  $S_w > 60\%$ ), whereas decreases much slowly in the low saturation range (e.g.  $S_w < 60\%$ ). A decrease of the  $w/c$  ratio results in the  $d_p$ -value to drop more rapidly. The  $d_p$ - $S_w$  plots of M5 ( $w/c = 0.5$ ) and M6 ( $w/c = 0.6$ ) are closer, compared to that of M4 ( $w/c = 0.4$ ).

The decrease of the  $d_p$ -value results in a lower amount of the water-filled pores and hence affects the ionic transport. In this respect more details will be given in the following Sects. 4.4 and 4.5.

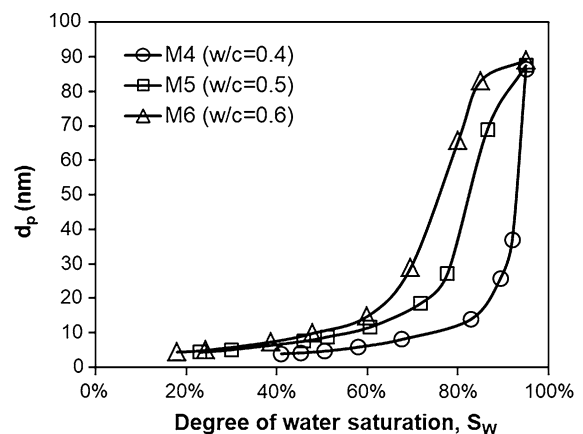


**Fig. 10** Moisture distribution, i.e.  $d_p$ - $S_w$  plots, estimated from the water vapour desorption isotherm tests of cement mortars (1 year old).  $d_p$  ( $d_p = 2r_p$ ) is the smallest drained pore diameter determined by Eq. (6)



#### 4.4 Relationship between relative chloride diffusion coefficient and water saturation

##### 4.4.1 Comparison of $D_{rc}$ - $S_w$ relationship between this study and previous studies

The available data ( $D_{rc}$  vs.  $S_w$ ) from the literature are also plotted in Fig. 7 for a comparative analysis. Based on the Nernst–Einstein equation and conductivity technique, Olsson et al. [13] determined the  $D_{rc}$ - $S_w$  relations in the cement mortars with  $w/c$  ratios of 0.38 and 0.53. Between the study of Olsson et al. and this study, the data are not very different for high saturation  $S_w$  levels, whereas disagreements arise for low saturation levels. In contrast to this study, Olsson et al. [13] concluded that the  $w/c$  ratio had little effect on the  $D_{rc}$ - $S_w$  relation in the OPC mortars. The different conclusions, drawn from different experimental results, might possibly be ascribed to two aspects: (1) the size and the age of the samples prior to the sample preconditioning procedures were different between the study of Olsson et al. and this study, and (2) the sample preconditioning approaches used were different, i.e. “RH” preconditioning was used by Olsson et al. while “SD” preconditioning was used in this study. Note that it is increasingly difficult for the “RH” preconditioning approach to prepare a sample with lower equilibrium moisture content. Therefore for low saturation levels, the moisture distributions of the samples obtained from the “RH” preconditioning approach may exhibit great differences from those of the samples obtained from the “SD” preconditioning approach.

Besides the OPC binder, three blended binders were also prepared by Olsson et al. [13] to study the ionic diffusion under non-saturated state. The topic on the effect of various blended materials on the  $D_{rc}$ - $S_w$  relation is beyond the scope of this work. The details will be discussed in a separate paper.

The values of critical saturation  $S_{cr}$  from the literature are compared with those derived in this study. Martys [50] simulated the non-saturated ionic diffusion in wetting fluid by means of lattice Boltzmann method. He found that a connected water-filled path can be formed allowing for ionic diffusion only when the water saturation was above 0.33. Based on the diffusion tests, de Vera et al. [51] measured the chloride diffusion coefficients of the cement concretes with interior RH of 54, 75, 86 and > 95%. It was

found that a lower  $w/c$  ratio resulted in a higher  $S_{cr}$ -value, a similar trend as presented in this study. On the other hand, de Vera et al. [51] reported critical saturations  $S_{cr} = 0.4$  and  $S_{cr} = 0.33$  for the cement concretes with  $w/c = 0.5$  and  $w/c = 0.6$ , respectively. The  $S_{cr}$ -values from de Vera et al. are higher than those derived in this study. This possibly results from the fact that de Vera et al. applied the “RH” preconditioning approach to prepare concrete samples, while in this study the “SD” preconditioning approach was used to prepare mortar samples.

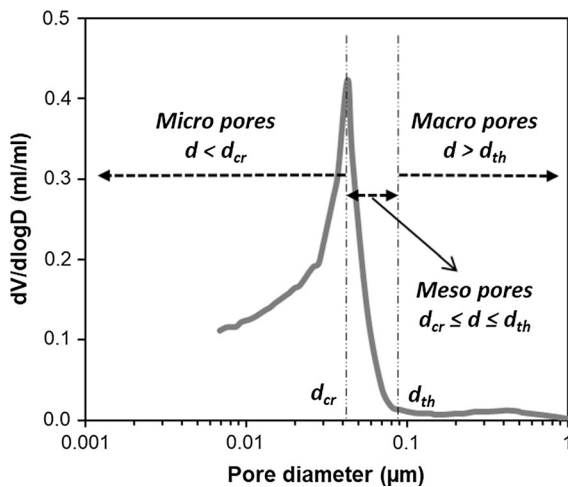
##### 4.4.2 $D_{rc}$ - $S_w$ relationship and moisture distribution

Figure 7 has shown that the relative chloride diffusion coefficient  $D_{rc}$  is highly dependent on the degree of water saturation  $S_w$ . The decrease of the  $D_{rc}$ -value with decreasing  $S_w$  can be ascribed primarily to three aspects: (1) the amount of water available for the chloride diffusion is less; (2) the number of transport channels, where continuous water-filled paths are present, becomes less; (3) the interaction forces between chloride ions and cement paste are increased due to the decreased thickness of the water layers adsorbed on the pore walls [52].

The three aspects mentioned above are, in essence, related to the moisture state in the pores. In a partially saturated porous system, there are three typical moisture states in a pore: saturated, partially saturated or drained (only adsorbed water film is present). It is sensible to assume that the saturated pores play a major role in the ionic transport. The moisture state in the entire capillary pores, i.e. moisture distribution, governs the relationship between  $D_{rc}$  and  $S_w$ .

For the sake of describing the moisture distribution, two pore parameters are introduced: threshold diameter and critical diameter [53]. Both are the key parameters influencing the pore connectivity. The threshold diameter ( $d_{th}$ ) corresponds to the pore size, above which there is comparably little mercury intrusion, immediately below which significantly intruded mercury is detected. The critical diameter ( $d_{cr}$ ) corresponds to the pore size, at which the mercury can fill the bulk of the specimen. Based on the pore size distribution obtained from the MIP test, the pore size can be categorized into three groups (Fig. 11): (1) macro pores, with diameter  $d > d_{th}$ ; (2) meso pores,  $d_{th} \geq d \geq d_{cr}$ ; (3) micro pores,  $d < d_{cr}$ .





**Fig. 11** Illustration of three pore size groups based on the pore size distribution of cement paste (1 year old,  $w/c = 0.5$ ) obtained from the MIP test.  $d_{th}$  and  $d_{cr}$  refer to threshold diameter and critical diameter, respectively

The macro pores refer to the large void space present in the surface specimen, which will be filled with mercury at the beginning of the MIP test. When a threshold pressure corresponding to the threshold diameter  $d_{th}$  is applied, the mercury starts to fill the small void space present in the surface specimen and penetrate rapidly into the specimen with increasing pressure. Once the critical pores (diameter  $d_{cr}$ ) are filled, a connected pore network forms and the mercury fills the bulk specimen. The meso pores, which are in the size range between  $d_{th}$  and  $d_{cr}$ , control the percolation of the pore structure, and they represent the void space within the clusters of the loosely packed hydrates. With further increase of the applied pressure the mercury penetrates the micro pores, which account for the void space within the clusters of the densely packed hydrates.

On basis of the mercury penetration in the microstructure of hydrated cementitious system, a simple pore network as shown in Fig. 12 can be extracted. The micro pores and macro pores are both connected through the meso pores. When the pore system is partially saturated, the meso pores provide the main pathways for moisture transfer, and the moisture loss in meso pores will significantly influence the continuity of water-filled pores. According to the Kelvin law, with a decrease of water saturation the water in the pore network gradually loses from the macro pores to the micro pores. Water loses in a pore

until the pore is only adsorbed with a thin water film [29]. Impedance spectroscopy measurements, conducted by Sánchez et al. [54], confirmed that all the pores kept at least a thin layer of electrolyte covering their walls, regardless of the saturation levels ( $S_w = 18\text{--}100\%$ ).

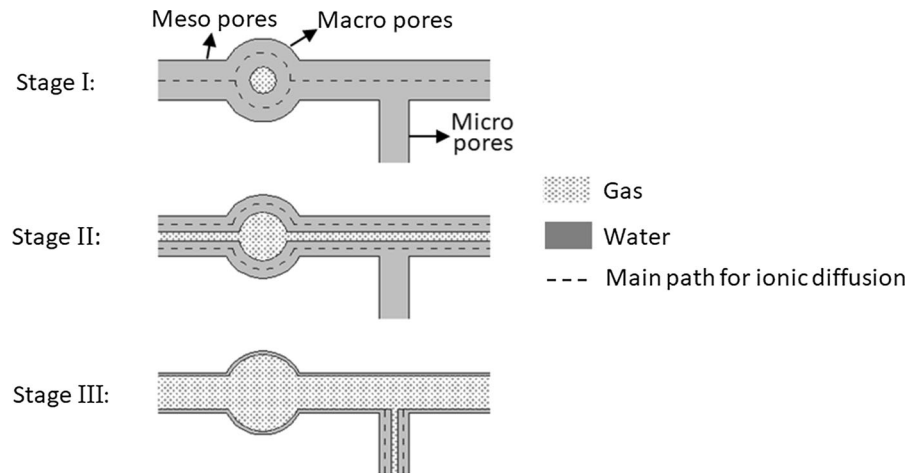
The three-stage  $D_{rc}\text{--}S_w$  relationship (see Fig. 7) can be explained by the three-stage change of the moisture state in the meso pores (see Fig. 12):

- *Stage I* All the meso pores are saturated. When the  $S_w$  starts to decrease from fully saturated state, the macro pores lose water. The main pathways for ionic diffusion, viz. meso pores, remain filled with water. The  $D_{rc}$ -value is not much influenced and quite close to that in the saturated condition.
- *Stage II* With further decrease of the  $S_w$  level, the meso pores start to lose water and become partially saturated. In the meantime the meso pores are gradually occupied with the gas phase, which can hinder the ionic diffusion to a great extent. As a result, the  $D_{rc}$ -value drops rapidly.
- *Stage III* Once the  $S_w$  is lower than a certain level, nearly all the meso pores are drained but only adsorbed with the nano-scale layers, which are composed of water molecules and chemical compounds, e.g.  $\text{Ca}(\text{OH})_2$ . In this stage, the water loss commences in the micro pores. The ionic diffusion tends to be quite slow and the  $D_{rc}$ -value decreases less obviously.

#### 4.5 Role of $w/c$ ratio in relative chloride diffusion coefficient

The role of the  $w/c$  ratio in the  $D_{rc}\text{--}S_w$  relation is a result of its effect on the moisture distribution in the pore structure. The moisture distribution, in essence, determines the number of transport channels, where the water-filled pores are connected and ionic diffusion can take place. At a particular water saturation  $S_w$ , the amount of water-filled pores and their continuity can be altered with varying  $w/c$  ratios. The term *water continuity* is introduced to quantify the effect of moisture distribution on the number of transport channels.

**Fig. 12** Schematic representations of the moisture distribution and ionic diffusion in the pore network with decreasing water saturation level



#### 4.5.1 Definition of water continuity

The water continuity  $\eta_w$  indicates the continuity of water-filled pores in a porous system. A channel that consists of continuous water-filled pores allows for ionic transport. The water continuity is expressed as:  $\eta_w = N_w/N_{Sat}$ , where  $N_w$  and  $N_{Sat}$  represent the number of transport channels available for ionic transport when the porous system is at a particular water saturation level and at saturated state, respectively. At saturated state, all the connected pores are filled with water allowing for ionic transport, i.e.  $N_w = N_{Sat}$  and  $\eta_w = 1$ . A decrease of the water saturation leads to a decrease of the  $N_w$ -value and hence a decrease of the  $\eta_w$ -value. When the water saturation is lower than a critical level, there is no continuous water-filled path allowing for ionic transport, i.e.  $N_w = 0$  and  $\eta_w = 0$ . A decrease of the water continuity  $\eta_w$  results in a decrease of the relative chloride diffusion coefficient  $D_{rc}$ .

#### 4.5.2 Role of $w/c$ ratio in water continuity

The role of the  $w/c$  ratio in water continuity can be evaluated by two different ways. One way is based on the water vapour desorption isotherm (i.e.  $d_p$ - $S_w$  plots, see Fig. 10), and the other way is based on the pore connectivity of the specimen.

In partially saturated specimens, the transport channels are constituted mainly by the water-filled pores (with diameter  $d \leq d_p$ ). A decrease of the water saturation  $S_w$  results in a decrease of the  $d_p$ -value. For the cement mortar with a lower  $w/c$  ratio, the  $d_p$ -value

decreases more rapidly with the decreasing water saturation (see Fig. 10). In principle, a greater decrease in the  $d_p$ -value leads to a greater decrease in the number of transport channels ( $N_w$ -value). It is considered, therefore, that at the same water saturation level the water continuity  $\eta_w$  and associated  $D_{rc}$ -value can be smallest in the mortar M4, followed by M5 and M6 in a larger order. The closer  $d_p$ - $S_w$  plots of M5 and M6, as seen from Fig. 10, provide an evidence for their similar  $\eta_w$ -values. All these are in good agreement with the  $D_{rc}$ - $S_w$  relations shown in Fig. 7.

Alternatively, the water continuity  $\eta_w$  is evaluated from the pore connectivity point of view. With declining water saturation  $S_w$ , the continuity  $\eta_w$  of water-filled pores will be less severely influenced in the specimen with higher pore connectivity [55]. In this work the pore connectivity was estimated from the MIP tests, and it was determined as 44.2, 56.5 and 62.5% for the cement pastes with  $w/c$  ratios of 0.4, 0.5 and 0.6, respectively. Obviously, the pore connectivities at  $w/c = 0.5$  and  $w/c = 0.6$  differ a little, but both are much higher than the pore connectivity at  $w/c = 0.4$ . In this sense, for a given saturation  $S_w$  level, the water continuities  $\eta_w$  between M5 and M6 are more similar but both are much higher than that of M4. This provides a further evidence for the role of the  $w/c$  ratio in the  $D_{rc}$ - $S_w$  relations as presented in Fig. 7.

## 5 Conclusions

From the findings of this study, the following main conclusions can be drawn:

1. At a particular degree of water saturation  $S_w$ , the cement mortar with a higher  $w/c$  ratio shows a higher RH level. In the range of 50–90% RH, linear RH– $S_w$  relationships are observed for all the  $w/c$  ratios of 0.4, 0.5 and 0.6.
2. The change of relative chloride diffusion coefficient  $D_{rc}$  with decreasing saturation  $S_w$  level can be divided into three stages, i.e. a slight decrease (stage I), a sharp drop (stage II) and another slight decline (stage III).
3. The  $w/c$  ratio plays an important role in both water vapour desorption isotherm and  $D_{rc}$ – $S_w$  relationship. This indicates that the  $D_{rc}$  in unsaturated cementitious material strongly depends on the microstructure of the material. At a particular water saturation  $S_w$ , the  $D_{rc}$  is larger for a higher  $w/c$  ratio. However, the role of the  $w/c$  ratio in the  $D_{rc}$ – $S_w$  relation becomes less pronounced with increasing  $w/c$  ratio.
4. There exists a critical saturation level, below which the water-filled capillary pores are unable to form a continuous path to allow for ionic diffusion. The  $w/c$  ratio has a great influence on the critical saturation. The critical saturation levels for the 370-day OPC mortars with  $w/c$  ratios of 0.4, 0.5 and 0.6 are found to be 37, 28 and 22%, respectively.
5. A finer pore size distribution or lower pore connectivity tends to result in a smaller relative chloride diffusion coefficient  $D_{rc}$ .

**Acknowledgements** The first author would like to thank Na Zhang for the experimental analysis. The support from the technicians in the Microlab of Delft University of Technology is highly appreciated. The funding from China Scholarship Council (CSC) is gratefully acknowledged.

**Funding** This study was funded by China Scholarship Council (Grant Number 2010695028).

#### Compliance with ethical standards

**Conflict of interest** The authors declare that they have no conflict of interest.

**Open Access** This article is distributed under the terms of the Creative Commons Attribution 4.0 International License (<http://creativecommons.org/licenses/by/4.0/>), which permits unrestricted use, distribution, and reproduction in any medium, provided you give appropriate credit to the original

author(s) and the source, provide a link to the Creative Commons license, and indicate if changes were made.

#### References

1. Tuutti K (1982) Corrosion of steel in concrete. Dissertation, Lund University
2. DuraCrete R17 (2000) DuraCrete final technical report, The European Union—Brite EuRam III, DuraCrete—probabilistic performance based durability design of concrete structures, document BE95-1347/R17, CUR, Gouda, The Netherlands
3. Zhang Y, Ye G (2016) Development of interior relative humidity due to self-desiccation in blended cementitious system. In: International RILEM conference on materials, systems and structures in civil engineering conference segment on moisture in materials and structures, Lyngby, Denmark, pp 341–350
4. Chatterji S (1994) Migration of ions through cement based materials Part I. *Cem Concr Res* 24:907–912
5. Chatterji S (2004) An explanation for the unsaturated state of water stored concrete. *Cem Concr Compos* 26:75–79
6. Zhang Y, Zhang M (2014) Transport properties in unsaturated cement-based materials—a review. *Constr Build Mater* 72:367–379
7. Climent MA, de Vera G, Lopez JF, Viqueira E, Andrade C (2002) A test method for measuring chloride diffusion coefficients through non-saturated concrete. Part I: the instantaneous plane source diffusion case. *Cem Concr Res* 37:714–724
8. Nielsen EP, Geiker MR (2003) Chloride diffusion in partially saturated cementitious material. *Cem Concr Res* 33:133–138
9. Guimarães ATC, Climent MA, de Vera G, Vicente FJ, Rodrigues FT, Andrade C (2011) Determination of chloride diffusivity through partially saturated Portland cement concrete by a simplified procedure. *Constr Build Mater* 25:785–790
10. Climent MA, Viqueira E, de Vera G, López-Atalaya MM (1999) Analysis of acid-soluble chloride in cement, mortar, and concrete by potentiometric titration without filtration steps. *Cem Concr Res* 29:893–898
11. Mercado-Mendoza H, Lorente S, Bourbon X (2014) Ionic aqueous diffusion through unsaturated cementitious materials—A comparative study. *Constr Build Mater* 51:1–8
12. Mercado-Mendoza H, Lorente S, Bourbon X (2013) The diffusion coefficient of ionic species through unsaturated materials. *Transp Porous Med* 96:469–481
13. Olsson N, Baroghel-Bouny V, Nilsson LO, Thiery M (2013) Non-saturated ion diffusion in concrete—a new approach to evaluate conductivity measurements. *Cem Concr Compos* 40:40–47
14. Zhang Y, Ye G (2015) Chloride transport in partially saturated mortar made of blended cement. In: Proceedings of the 14th international congress on the chemistry of cement (ICCC2015). Beijing, China
15. Zhang Y, Ye G (2014) Chloride diffusivity in partially saturated cement-based materials assessed by resistivity



- measurements. In: Proceedings of service life design for infrastructure. Zhuhai, China
16. Zhang Y, Ye G (2017) A mathematical model in characterizing chloride diffusivity in unsaturated cementitious materials. In: 1st international conference on construction materials for sustainable future, Zadar
  17. Zhang M, Ye G, van Breugel K (2012) Modeling of ionic diffusivity in non-saturated cement-based materials using lattice Boltzmann method. *Cem Concr Res* 42:1524–1533
  18. DIN 50008 (1981) Part 1. standard atmospheres over aqueous solutions Deutsches Institut für Normung (DIN). Berlin, Germany
  19. Antón C, Climent MA, de Vera G, Sánchez I, Andrade C (2013) An improved procedure for obtaining and maintaining well characterized partial water saturation states on concrete samples to be used for mass transport tests. *Mater Struct* 46:1389–1400
  20. Åhs M, Nilsson LO, Haha MB (2015) A method to determine the critical moisture level for unsaturated transport of ions. *Mater Struct* 48:53–65
  21. Ye G (2003) Experimental study and numerical simulation of the development of the microstructure and permeability of cementitious materials. Dissertation, Delft University of Technology
  22. Diamond S (2000) Mercury porosimetry: an inappropriate method for the measurement of pore size distributions in cement-based materials. *Cem Concr Res* 30:1517–1525
  23. Kaufmann J, Loser R, Leemann A (2009) Analysis of cement-bonded materials by multi-cycle mercury intrusion and nitrogen sorption. *J Colloid Interface Sci* 336:730–737
  24. Washburn EW (1921) The dynamics of capillary flow. *Phys Rev* 17:273–283
  25. Garboczi EJ (1990) Permeability, diffusivity and microstructural parameters: a critical review. *Cem Concr Res* 20:591–601
  26. Brunauer S (1943) The adsorption of gases and vapors, vol I. Physical adsorption. Princeton University Press, Princeton
  27. Fisher LR (1981) Experimental studies on the applicability of the Kelvin equation to highly curved concave menisci. *J Colloid Interface Sci* 80:528–541
  28. Neimark AV, Ravikovitch PI, Vishnyakov A (2003) Bridging scales from molecular simulations to classical thermodynamics: density functional theory of capillary condensation in nano pores. *J Phys: Condens Matter* 15:347–365
  29. Badmann R, Stockhausen N, Setzer MJ (1981) The statistical thickness and the chemical potential of adsorbed water films. *J Colloid Interface Sci* 82:534–542
  30. Lu XY (1997) Application of the Nernst-Einstein equation to concrete. *Cem Concr Res* 27:293–302
  31. McKee RA (1981) A generalization of the Nernst-Einstein equation for self-diffusion in high defect concentration solids. *Solid State Ionics* 5:133–136
  32. Rajabipour F, Weiss J (2007) Electrical conductivity of drying cement paste. *Mater Struct* 40:1143–1160
  33. Weast RC (1976) Handbook of chemistry and physics, 57th edn. CRC Press, Cleveland
  34. Polder RB (2000) Test methods for onsite measurement of resistivity of concrete—a RILEM TC-154 technical recommendation. *Constr Build Mater* 15:125–131
  35. Parrott LJ (1994) Moisture conditioning and transport properties of concrete test specimens. *Mater Struct* 27:460–468
  36. Panea I, Hansen W (2005) Investigation of blended cement hydration by isothermal calorimetry and thermal analysis. *Cem Concr Res* 35:1155–1164
  37. Gallé C (2001) Effect of drying on cement based materials pore structure as identified by mercury intrusion porosimetry—a comparative study between oven, vacuum and freeze drying. *Cem Concr Res* 31:1467–1477
  38. Feldman RF, Beaudoin JJ (1991) Pre-treatment of hardened hydrated cement pastes for mercury intrusion measurements. *Cem Concr Res* 21:297–308
  39. Taylor HFW (1997) Cement chemistry, 2nd edn. Academic Press Thomas Telford, London
  40. Winslow DN, Liu D (1990) The pore structure of paste in concrete. *Cem Concr Res* 20:227–235
  41. Murat M (1982) Stabilité thermique des aluminates de calcium hydratés et phases apparentées. Caractérisation par les méthodes thermoanalytiques. Aluminates Calcium, Int Semin, Turin, Italy, pp 59–84
  42. Aono Y, Matsushita F, Shibata S, Hama Y (2007) Nanostructure changes of C-S-H in hardened cement paste during drying at 50 °C. *J Adv Concr Technol* 5(3):313–323
  43. RILEM TC 116-PCD (1999) Recommendations: a pre-conditioning of concrete test specimens for the measurement of gas permeability and capillary absorption of water. *Mater Struct* 32:174–176
  44. Baquerizo L (2015) Impact of water activity on the mineralogy of hydrated cement. Dissertation, Swiss Federal Institute of Technology
  45. Ramachandran VS, Beaudoin JJ (2001) Handbook of analytical techniques in concrete science and technology principles, techniques, and applications. Noyes/William Andrew, New York
  46. Snyder KA, Feng X, Keen BD, Mason TO (2003) Estimating the electrical conductivity of cement paste pore solutions from OH<sup>-</sup>, K<sup>+</sup> and Na<sup>+</sup> concentrations. *Cem Concr Res* 33:793–798
  47. Taylor HFW (1987) A method for predicting alkali ion concentrations in cement pore solutions. *Adv Cem Res* 1:5–16
  48. Chen W, Brouwers HJH (2010) Alkali binding in hydrated Portland cement paste. *Cem Concr Res* 40:716–722
  49. Zhang Q (2013) Microstructure and deterioration mechanisms of Portland cement paste at elevated temperature. Dissertation, Delft University of Technology
  50. Martys NS (1999) Diffusion in partially-saturated porous materials. *Mater Struct* 32:555–562
  51. De Vera G, Climent MA, Viqueira E, Antón C, Andrade C (2007) A test method for measuring chloride diffusion coefficients through partially saturated concrete. Part II: the instantaneous plane source diffusion case with chloride binding consideration. *Cem Concr Res* 37:714–724
  52. Saetta AV, Scotta RV, Vitaliani RV (1993) Analysis of chloride diffusion into partially saturated concrete. *ACI Mater J* 90(5):441–451
  53. Aligizaki KK (2006) Pore structure of cement-based materials: testing, interpretation and requirements. CRC Press, Boca Raton

- 
54. Sánchez I, Antón C, de Vera G, Ortega JM, Climent MA (2013) Moisture distribution in partially saturated concrete studied by impedance spectroscopy. *J Nondestruct Eval* 32:362–371
55. Zhang M, Xu K, He Y, Jivkov AP (2014) Pore-scale modelling of 3D moisture distribution and critical saturation in cementitious materials. *Constr Build Mater* 64:222–230